Waste Biomass Valor (2014) 5:293–304
DOI 10.1007/s12649-013-9245-8

ORIGINAL PAPER

Anaerobic Biodegradation of Cellulose–Xylan–Lignin Nanocomposites as Model Assemblies of Lignocellulosic Biomass

Abdellatif Barakat · Cédric Gaillard · Jean-Philippe Steyer · Hélène Carrere

Received: 24 October 2012 / Accepted: 11 May 2013 / Published online: 24 May 2013

Abstract In order to determine the parameters influencing lignocellulosic biomass biodegradability, binary and ternary model systems were constructed, consisting of cellulose nanowhiskers gel, xylan matrix derived from lignocellulosic plants and synthetic lignin. The adsorption of two xylan polymers with different arabinose/xylose ratios (Ara/Xyl) on the cellulose nanowhiskers resulted in the synthesis of nanocomposites each of different Ara/Xyl ratios and crystallinity indexes. Organized and associated cellulose–xylan–lignin nanocomposites were formed following the polymerization of guaïacyl (G) and syringyl (S) lignin monomers using a peroxidase/H_2O_2 system in cellulose nanowhiskers-xylan gel. The anaerobic digestion of cellulose nanowhiskers, xylans and cellulose–xylan nanocomposites indicated that the biomethane production depended strongly on the xylan Ara/Xyl ratio and on the cellulose crystallinity. However, the anaerobic digestion of cellulose–xylan–lignin nanocomposites showed that the digestion rate decreased significantly in the presence of lignin. Moreover, there was an even more considerable decrease in digestion rate in the presence of GS-type lignin compared to G-type lignin.

A. Barakat · J.-P. Steyer · H. Carrere (✉)
INRA, UR0050, Laboratoire de Biotechnologie de l'Environnement, Avenue des Etangs, 11100 Narbonne, France
e-mail: helene.carrere@supagro.inra.fr

A. Barakat
INRA, UMR 1208 Ingénierie des Agropolymères et Technologies Emergentes (UMR IATE), 2, place Pierre Viala, 34060 Montpellier cedex 1, France

C. Gaillard
INRA, UR 1268 BIA, Laboratoire de Microscopies, Plateforme BIBS, rue de la Géraudière B.P. 71627, 44316 Nantes Cedex 03, France

Keywords Anaerobic digestion · Biogas · Accessibility · Plant cell wall · Lignocellulosic materials · Model assemblies

Abbreviations

Ara	Arabinose
BMP	Biomethane potential
Carb	Carbohydrates
CrI	Crystallinity Index
L	Lignin
LG	Guiacyl lignin
LGS	Guiacyl-syringyl lignin
Lm	Lignin monomers
XY	Xylan
Xyl	Xylose
XYm	Xylan polymer with Ara/Xyl = 0.32
XYs	Xylan polymer with Ara/Xyl = 0.12
VFA	Volatile fatty acids
WS	Cellulose whiskers
WS-XY	Whiskers-xylans assemblies
WS-XY-L	Whiskers-xylans-lignin assemblies
WS-XY-LG	Whiskers-xylans-lignin assemblies with guiacyl lignin
WS-XY-LGS	Whiskers-xylans-lignin assemblies with zguiacyl and syringyl lignin

Introduction

Lignocellulosic biomass is a promising alternative to limited crude oil and, in its place, can be utilized to produce renewable bioenergy and byproducts or biomaterials. Lignocellulosic plant cell walls consist mainly of cellulose, hemicelluloses and lignin. Cellulose consists of D-glucose subunits linked by β-(1 → 4) glycosidic bonds. The

cellulose in a plant consists of parts with an organized crystalline structure and parts with a poorly organized amorphous structure. The hemicelluloses are branched with short lateral chains that consist of different sugar monomers. Hemicelluloses serve as a connection between the lignin and the cellulose fibers and give rigidity to the whole cellulose–hemicellulose–lignin network [1]. In general, the dominant hemicelluloses in plant cell walls are xylans which display significant variability in their structural characteristics [2]. Lignin is an amorphous heteropolymer consisting of three different phenylpropane alcohols: *p*-coumaryl (H), coniferyl (G) and sinapyl (S) (Fig. 1) [3, 4]. The nature and the quantity of lignin monomers (H, G, S) vary according to species, maturity and the space localization in the cell [3]. The lignins from softwoods contain mainly guaïacyl units, those from hardwoods and grass mainly guaïacyl (G) and syringyl (S) units [5].

Bioenergy production from lignocellulosic biomass by anaerobic digestion is one of the major contributing factors towards a future sustainable bioenergy economy [6–8]. Indeed anaerobic digestion of lignocellulosic biomass produces a biogas, containing carbon dioxide and methane that can be used either as heat and electricity, as biofuel or as a substitute for natural gas. In this process, anaerobic microorganisms convert carbohydrates, including hemicelluloses (C5-sugars) and cellulose (C6-sugars), proteins and also lipids, to biogas. Some phenolic compounds can also be converted to biogas [9]. Anaerobic digestion is composed of four main steps: hydrolysis, acidogenesis, acetogenesis and methanogenesis. Each stage requires the activity of its own specific group of micro-organisms. In the case of carbohydrates, hydrolysis leads to soluble sugar monomers (glucose, xylose, arabinose, mannose…). Acidogenesis is the transformation of soluble sugar monomers into volatile fatty acids (VFA). During acetogenesis, VFA are transformed into acetate, CO_2 and H_2. Finally, methanogenesis is the conversion of acetate, CO_2 and H_2 to methane by archae. Thus, the final product of anaerobic digestion is biogas which consists mainly of methane (55–75 %) and CO_2 (25–45 %). Hydrolysis is known to be the rate-limiting step in anaerobic digestion of most solid substrates [10]. Furthermore, the low accessibility of fermentable sugars in lignocellulosic biomass by anaerobic microorganisms has been emphasized [11, 12] and numerous studies have focused on the development of pretreatments, as in bioethanol processes, to improve anaerobic digestion performance [11, 13]. Nevertheless, while the role of native lignocellulosic structural features on cellulose enzymatic attack has been studied, only the impact of biomass composition (i.e. lignin, cellulose and hemicellulose) has been taken into account and linked with anaerobic digestion performance [12, 14–16]. These studies reported negative linear correlations between biomass methane potential and lignin content [14, 15] or between the sum of both lignin and cellulose contents [15, 16]. More recently, a study based on various lignocellulosic

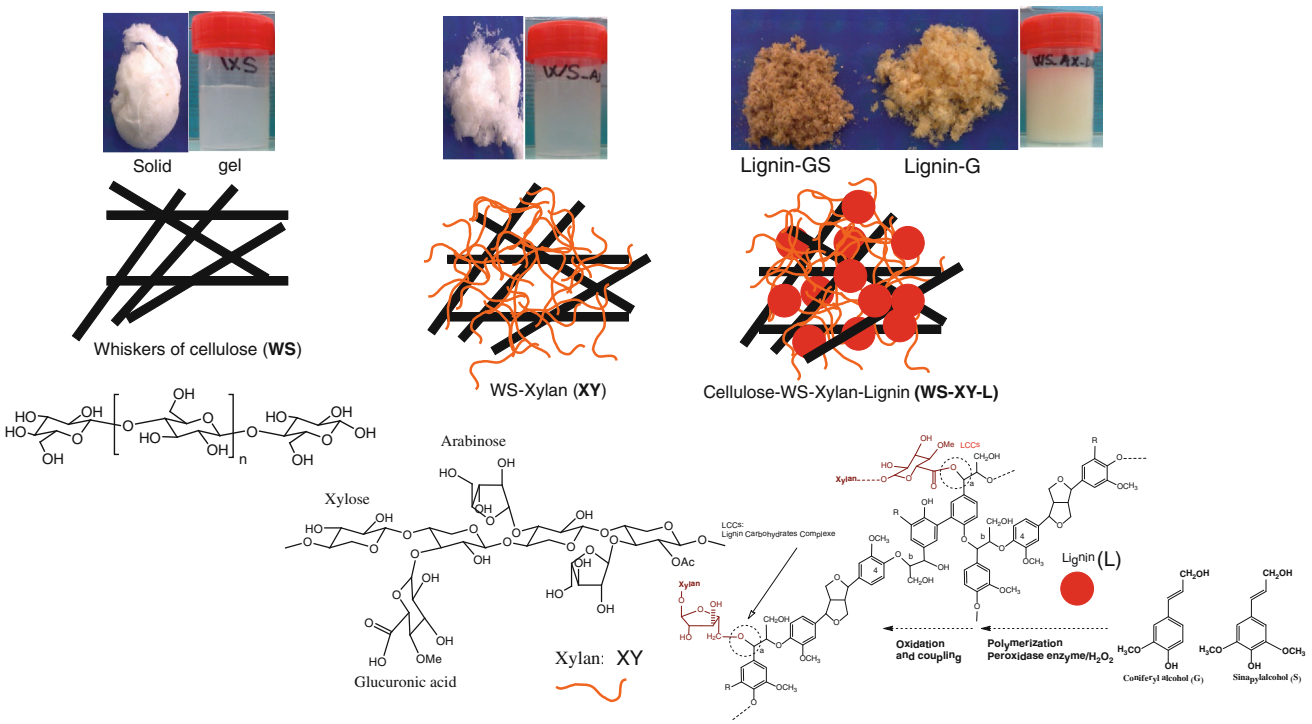

Fig. 1 Synthesis of whiskers-xylan "WS-XY" and whiskers-xylan-lignin "WS-XY-L" nanocomposites as models of lignocellulosic materials

substrates showed that methane potentials correlated negatively to the lignin contents and, to a lower extent, to crystalline cellulose content [12]. On the other hand, Benner et al. [17] reported that in the anaerobic digestion of grass after 294 days, 16.9 % of the lignin was degraded to gaseous end products, suggesting that lignin polymers do not inhibit anaerobic digestion and are slowly converted into biogas in the absence of oxygen. The enzymatic hydrolysis of pure cellulose has been proved to be influenced by the crystallinity of cellulose, their accessible surface area, protection by lignin, and cellulose–hemicelluloses–lignin association [18, 19]. Some works have shown a good correlation between crystallinity, surface properties, supramolecular structure and the rate of enzymatic hydrolysis in pure cellulose [20, 21]. Other works have reported that lignin polymer is the most recalcitrant component of the plant cell wall, and that the higher the proportion of lignin and aromatic compounds, the higher the resistance to chemical and enzymatic degradation [22, 23]. However, Rollin et al. [24] reported that increasing cellulose accessibility was a more important pretreatment consideration than delignification to effectively release sugars from recalcitrant lignocellulose at high yield. Indeed, all these results may be contradictory due to the very heterogeneous nature and complexity of lignocellulosic materials.

In order to better understand and determine the parameters influencing lignocellulosic accessibility and degradability, recent research has focused on the "model assemblies" of plant cell walls [25, 26]. For decades, the bacterium *Gluconoacetobacter* and commercial cellulose have been used as a matrix to study cellulose–hemicelluloses and cellulose–hemicelluloses–lignin organization and interactions. The resulting cellulose–hemicelluloses or bacterial cellulose–hemicelluloses–lignin composites have been widely investigated [27–30]. The originality of this present study includes the use of a nanowhiskers matrix (whiskers gel) as a polymerization medium and the production of a solid state complex involving cellulose–xylan and dehydrogenation polymers (DHP) as a lignin model. The synthesis of this cellulose–xylan-DHP was inspired from the synthesis of xylan-DHP assemblies [27–30].

The aim of this study was to investigate the impact of the structural feature of lignocellulosic materials (the crystallinity of cellulose, structure of hemicelluloses, lignin structure and content, cellulose–hemicelluloses–lignin association on the biodegradability of plant cell wall carbohydrates (C5 and C6-sugars) by anaerobic digestion. Therefore, various nanocomposites including cellulose–xylan, cellulose–lignin and cellulose–xylan–lignin were synthetized using different lignin structures (G- and GS-type lignin) and different xylan structures (different arabinose/xylose ratios). The methane potential and anaerobic digestion rate of these models were then analyzed and confronted with the characteristics of the model nanocomposites.

Materials and Methods

Xylan Polymers

The xylan polymers XYm and XYs were purchased from Megazyme and Sigma respectively.

Synthesis of Monolignols (Lignin Monomers)

Coniferyl alcohol (4-hydroxy-3-methoxy cinnamyl alcohol) and Sinapyl alcohol (4-hydroxy-3,5-methoxy cinnamyl alcohol) were obtained using the procedure described by Ludley and Ralph [31].

Synthesis of Cellulose Nanowhiskers (WS)

10 g of cellulose (11365-Avicel® PH-101 ~50 µm particle size) was hydrolyzed in 100 mL of HCl (70 %) at 60 °C for 30 min while being shaken vigorously. 100 mL of cold distilled water was added to stop the reaction. The diluted suspension was centrifuged at 10,000 rpm for 10 min to obtain the precipitate. The precipitate was again suspended in 200 mL of cold water, shaken vigorously, and was then centrifuged. This process was repeated until the supernatant became turbid (colloidal suspension). The colloidal suspension was collected and dialyzed against distilled water for 3 days. After 10 min of sonication treatment, the suspension (2 %) was stored at 4 °C.

Synthesis of Whiskers-Xylan Composites

Preparation conditions of the nanocomposites are reported in Table 1. The whiskers-xylan nanocomposites were prepared by adding about 0.5 g xylan to a 100 mL cellulose whiskers suspension (1.5 % w/v) and the reaction mixture was stirred for 24 h at 25 °C (Table 1).

Synthesis of Whiskers-Xylan-Lignin Composites

Three solutions were prepared for synthesis of the whiskers-xylan-lignin nanocomposites (Table 1). The polymerization reaction was carried out according to the "Zutropfverfahren method (ZT)"; 50 mL of solution B and 50 mL of C were gradually added to 100 mL of A, containing peroxidase (EC 1 11.1.7 purchased from Sigma 250–330 unit/mg) [25]. The reaction mixture was stirred for 10 h at 25 °C. A DeHydrogenation Polymer "DHP-G: lignin model" control was prepared through polymerization of coniferyl alcohol or Guaïacyl units (G) (without whiskers-xylan) in water.

Table 1 Synthesis conditions of whiskers-xylan and whiskers-lignin-xylan nanocomposites

Biocomposites	[Carb] (%) w/v		[Lm] (%) w/v		H_2O_2 (mL)	Unit of peroxidase[a]
	Solution A		Solution B		Solution C	
	[WS]	[XY]	S	G		
WS_{75}-XYs_{25}	1.5	0.5	0.0	0.0	0	0
WS_{75}-XYm_{25}	1.5	0.5	0.0	0.0	0	0
WS_{50}-XYs_{25}-LG_{25}	1.0	0.5	0.0	0.5	0.5	1,560–1,875
WS_{50}-XYs_{25}-$(LG_{50}S_{50})_{25}$	1.0	0.5	0.25	0.25	0.5	1,560–1,875
WS_{50}-XYm_{25}-LG_{25}	1.0	0.5	0.0	0.5	0.5	1,560–1,875
WS_{75}-LG_{25}	1.5	0.0	0.0	0.5	0.5	1,560–1,875

[a] Peroxidase (EC 1 11.1.7 purchased from Sigma 250–330 unit/mg)

Carb, Carbohydrates; WS, whiskers of cellulose; XY, Xylan; L, Lignin; Lm, Lignin monomers; S, Syringyl units; G, Guiacyl units

Microscopy

Transmission Electronic Microscopy (TEM)

A drop from each aqueous dispersion was first placed on a carbon-coated TEM copper grid (Quantifoil, Germany) and left to air-dry. The sample was then negatively stained with uranyl acetate (Merck, Germany). This was achieved by placing the sample-coated TEM grid successively on a drop of uranyl acetate aqueous solution (2 % w/w) and on a drop of distilled water. The grid was then air-dried before being introduced into the electron microscope. The samples were viewed using a JEOL JEM-1230 TEM (Jeol, Japan); this was operated at an acceleration voltage of 80 kV and equipped with a LaB6 filament. All the micrographs were recorded on a 1.35 K × 1.04 K × 12 bit ES500 W Erlangshen CCD camera (Gatan, USA).

Stereomicroscopy

A Leica M205FA stereomicroscope equipped with a 0.63 × planapochromatic objective and LED reflective illumination was used to visualize the whiskers-xylan-lignin nanocomposite before and after anaerobic digestion. 2,176 × 1,632 pixel sized images were acquired and saved as *.jpg files using a Peltier-cooled Leica DFC495 camera with the Leica ApplicationSuite (LAS) software core V3.5.0 (October 2009).

Carbohydrates Analysis and FTIR-ATR Measurements

The carbohydrate composition of lignocellulosic samples was measured using strong acid hydrolysis. The lignin content in the samples was determined using the Klason method. 10 mg of dried samples were treated with 72 % H_2SO_4 at ambient temperature for 1 h. The solutions were diluted with water to 12 % H_2SO_4 and autoclaved at 100 °C for 2 h. The hydrolysates were centrifuged at 10,000 rpm for 10 min. The Klason lignin content was determined as the weight of the residue. The supernatant was analyzed for sugars on high-pressure liquid chromatography (HPLC). HPLC analysis was used to quantify monosaccharides (glucose, xylose, arabinose). The analysis was carried out with a combined Water/Dionex system, using a BioRad HPX-87H column at 50 °C. The solvent was 0.005 M H_2SO_4 and flow rate at 0.3 mL/min. The recovery of monosaccharides was determined by standard addition (D-fucose) to the samples. A refractive index (RI) detector (Water) was used to quantify carbohydrates. The system was calibrated with glucose, xylose, and arabinose standards (Sigma-Aldrich). All samples (1 mL) were filtered through 0.22 μm filters before being measured. All the determinations reported here were the duplicate results.

All FTIR spectra were recorded in absorption mode at 4 cm^{-1} interval and 64 scans at room temperature. Spectra were collected in the 4,000–600 cm^{-1} range using a Nexus 5700 spectrometer (ThermoElectron Corp.) with built-in diamond ATR single reflection crystal and with a cooled MCT detector. Three spectra were recorded for each sample. All spectra pre-treatments were performed using Omnic v7.3. Since absorbance at 1,427 and 898 cm^{-1} is sensitive to the crystalline cellulose and amorphous cellulose respectively, the absorbance height ratio H_{1427}/H_{898} was used to determine cellulose crystallinity index (CrI). H_{1427}/H_{898} was calculated as a mean of 3 values from 3 spectra in Omnic v7.3 software with local baselines on each band.

Biomethane Potential (BMP) Tests

The substrates were digested in batch anaerobic flasks. The volume of each flask was 150 mL, with a working volume of 110 mL while the remaining 40 mL volume served as head space. Each flask was composed of: a macroelements solution (source of N, P, Mg, CA, and K….), an oligoelements

solution, a bicarbonate buffer solution and an anaerobic inoculum (5 g VS/L). Each flask was seeded with granular sludge from a mesophilic anaerobic digester in a sugar factory. The substrate to inoculum ratio was 0.2 gVS substrate/gVS inoculum, this low value assures that the biological system was not overloaded. Once the flasks were prepared, degasification was carried out with nitrogen in order to obtain anaerobic conditions and the bottles were closed with air impermeable red butyl rubber septum-type stoppers. Duplicate bottles were incubated at 35 °C. A blank test was carried without sample to measure endogenous methane production from the inoculum and this endogeneous methane production was subtracted from the methane production of all the samples. Biogas volume was monitored using the water displacement method and the corresponding cumulative biogas volume was calculated. Acidified water (pH = 2) was used to minimize the dissolution of carbon dioxide in the water. Biogas composition was determined using a gas chromatograph (Varian GC-CP4900) equipped with two columns. The first one (Molsieve 5A PLOT) was used at 110 °C to separate O_2, N_2 and CH_4. The second one (HayeSep A) was used at 70 °C to separate CO_2 from other gases. The injector temperature was at 110 °C and the detector at 55 °C. Detection of gaseous compounds was performed using a thermal conductivity detector. Calibration was carried out with a standard gas composed of 25 % CO_2, 2 % O_2, 10 % N_2 and 63 % CH_4.

The kinetics of methane production were modeled using a modified Gompertz equation $V(t) = V_{max} \exp\{-\exp\left[\frac{R_{max}.e}{P}(\lambda - t) + 1\right]\}$ where V_{max} is the maximal cumulated CH_4 production (mL gVS^{-1}), R_{max} is the maximum CH_4 production rate (mL gVS^{-1} day^{-1}), λ is lag-phase time (day), t is the incubation time (day) and e is exp(1).

Results and Discussion

In this study, whiskers-xylan-lignin nanocomposites were obtained through the polymerization of lignin monomers (coniferyl "G" and sinapyl "S" alcohols) in a whiskers-xylan suspension (Fig. 1; Table 1). The reaction mixtures were therefore composed of DeHydrogenation Polymer "DHP" from guaïacyl alone (LG_{100}), from guaïacyl and syringyl units ($LG_{50}S_{50}$) and from whiskers-xylan colloidal nanocomposites. Both xylan polymers used had different arabinose/xylose (Ara/Xyl) ratios (see Table 2 for details on XYm and XYs structure). Indeed ramification chains were reported to play a significant role in cellulose/xylan interactions. Polymerization proceeded according to the Zutropfverfharen (ZT) method in which the monomers and hydrogen peroxide (enzyme cofactor) were continuously added to a solution of polysaccharides containing the oxidative enzyme (peroxidase). Monolignols (coniferyl and sinapyl alcohols) were oxidized into radicals capable of reacting with other monolignols, with the growing lignin polymers, or with carbohydrates (Fig. 1). The formation of whiskers-xylan-lignin nanocomposites was confirmed by the formation of stable colloïdal suspensions. Part of the suspensions was freeze-dried for anaerobic digestion and characterization.

Table 2 Biochemical composition and crystallinity index of cellulose nanowhiskers, xylan, and nanocomposites

Composition	CEL (%)	XY (%)	L (%)	Ara/Xyl	H_{1427}/H_{898}
WS	100	–	–	–	0.88
XYs	–	100	–	0.12	–
XYm	–	100	–	0.32	–
WS_{75}-XYs_{25}	77.8	22.2	–	0.13	1.08
WS_{75}-XYm_{25}	79.9	20.1	–	0.31	0.82
WS_{75}-LG_{25}	78.9	–	21.1	–	0.45
WS_{50}-XYm_{25}-LG_{25}	57.7	20.7	21.6	0.28	0.59
WS_{50}-XYm_{25} $(LG_{50}S_{50})_{25}$	58.6	20.4	21.0	0.26	0.50
WS_{50}-XYs_{25}-LG_{25}	56.8	21.8	21.4	0.08	0.70
LG_{100}	–	–	100	–	–

WS whiskers of cellulose, *CEL* cellulose, *XY* xylan, *L* lignin, *Ara/Xyl* arabinose/xylose ratio, *S* syringyl units, *G* guiacyl units

Characterization of Samples

Transmission Electronic Microscopy

The negative stained TEM (Fig. 2) revealed that the nanowhiskers produced were nanostructured microfibrils and exhibited a length of around 300 nm. The nanocomposites formed in the presence of xylan and lignin (Fig. 2) presented a different architecture. This structure showed considerable heterogeneity, with very dense regions in which the bundles were covered with xylan and lignin aggregates. The size of the lignin nodules present in WS-XY-LG nanocomposites was about 150 nm which was of the same order as those of natural lignin (≤100 nm) [32]. Similar shapes and sizes have already been reported for lignin nodules dispersed in polysaccharide suspensions [25, 30]. WS-XY-L nanocomposites displayed a dense structure and interconnected matrix, revealing evidence of an interaction between whiskers-xylan and lignin. TEM images clearly indicate the incorporation of spherical-formed lignin nodules into cellulose nanowhiskers microfibrils (Fig. 2).

Biochemical Composition

Carbohydrate and lignin contents in the nanocomposite samples are presented in Table 2. The chemical

composition of these WS-XY-L model assemblies presents the same composition as natural plant cell walls (~35–55 % cellulose, ~15–25 % hemicelluloses and ~15–25 % lignin). The synthetic lignin and xylan ratios in nanocomposites were different when compared to the amount of lignin monomers and xylans used (Table 1). It appeared that an amount of lignin and xylan was lost during the washing of nanocomposites after freeze drying. As can be seen in Table 2, lignin content was similar in WS-LG, WS-XY-LG and WS-XY-LGS nanocomposites. In contrast, the general trend for both WS-XY and WS-XY-L nanocomposites, was an increased level of the incorporation of xylan into the cellulose with decreasing Ara/Xyl ratios (Table 2), indicating a preferential adsorption of low substituted xylans. It may be possible that the lower arabinose content favored the aggregation of xylans and as a consequence caused the retention of larger particles within the nanowhiskers [33]. It also becomes obvious that XYs xylan (Table 2) had stronger interactions with nanowhiskers than those of XYm. After lignification, a

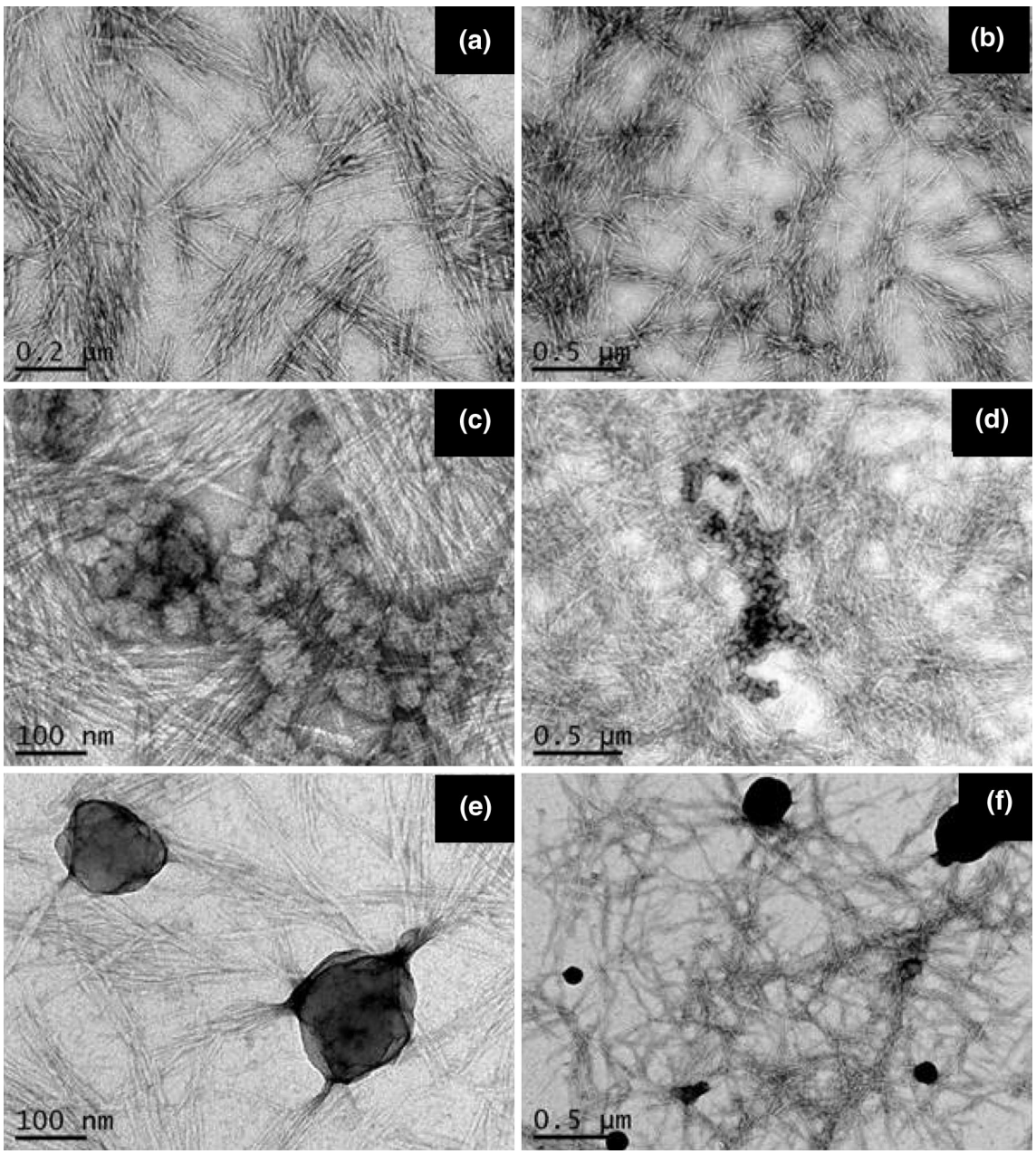

Fig. 2 Negative stained TEM micrographs of: **a**, **b** whiskers; **c**, **d** whiskers-xylan; and **e**, **f** whiskers-xylan-lignin nanocomposites. Images a, **c**, **d** correspond to higher magnification views of images **b**, **d**, and **f** respectively

decrease in the Ara/Xyl ratio revealed that there was some incorporation of xylan in the lignin matrix. It has been reported that arabinose can be added to nucleophilic groups on the transient quinone methide intermediate generated during the oxidative polymerization of lignin [34, 35]. These results clearly indicate that the incorporation and the association of xylan chains and lignin to cellulose nanowhiskers led to the formation of a nanostructured composite and confirmed the TEM observations (Fig. 2).

Infrared Spectroscopy

In order to further investigate the physicochemical structures of WS-LG, WS-XY-LG and WS-XY-LGS nanocomposites, FTIR spectra were recorded as shown in Fig. 3. The corresponding bands and the assignments are listed in Table 3 according to published data [36, 37]. The band at 1,510 cm^{-1} (aromatic skeletal vibrations) was used as a reference for lignin. The peaks at 1,369, 1,048 and 898 cm^{-1} are mainly due to carbohydrates and have no significant contribution from lignin [37]. Figure 4 shows the appearance of bands at 1,510, 1,269 and 1,210 cm^{-1}, in the case of WS-LG, WS-XY-LG and WS-XY-LGS, proving the incorporation of lignin in nanocomposites (Fig. 3 a–c). However, many differences appear among the spectra of all the samples in the fingerprint region between 1,800 and 800 cm^{-1}. This suggests that the xylan and lignin structure had an effect on WS-XY-L supramolecular structure. For example, the increase in bands at 1,210 and 1,336 cm^{-1} and the decrease in bands at 1,269 cm^{-1} proved the presence of lignin-GS. This further certifies that WS-XYs-LGS lignin is a GS-type lignin and thus different from WS-XYs-LG lignin (G-type lignin). WS-XYs-LGS and WS-XYs-LG assemblies can consequently be used as models for both grass and woody plants.

Table 2 shows the H_{1427}/H_{898} ratios of cellulose nanowhiskers (0.88), whiskers-xylans nanocomposites (0.82 and 1.08), and whiskers-xylans-lignin nanocomposites (ranging from 0.47 to 0.70). The H_{1427}/H_{898} ratio of initial Avicel microcrystalline cellulose was 1.48. This indicates that cellulose nanowhiskers produced had both crystalline and amorphous fractions. In addition, a modification of cellulose crystallinity resulted from xylan and lignin incorporation. The WS-XYs, WS and WS-XYm nanocomposites had the higher *CrI* and WS-LG, WS-XYm-LGS and WS-XYm-LG nanocomposites had the lowest *CrI*. This agrees with the general finding that the adsorption of amorphous polymers on cellulose microfibrils decreases cellulose crystallinity [29]. The lignin-GS type sample also had a greater effect than the lignin-G type.

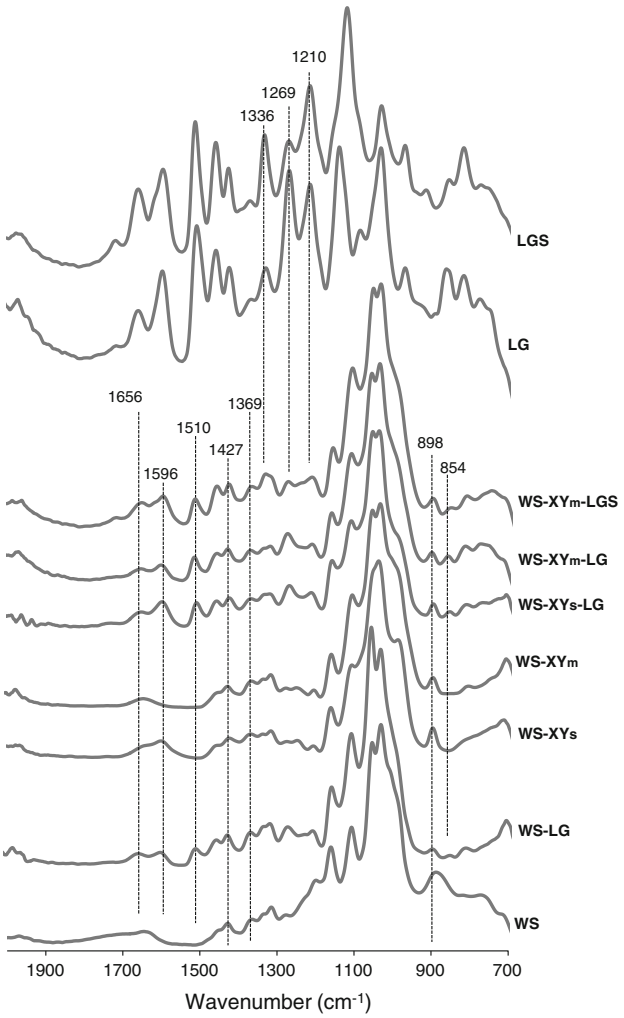

Fig. 3 FTIR absorbance spectra of whiskers of cellulose (WS), whiskers-xylans nanocomposites (WS-XY), and whiskers-xylans-lignin nanocomposites (WS-XY-LG) with LG: guiacyl lignin and LGS guiacyl and syringyl lignin

Batch Anaerobic Digestion

Influence of Xylan and Cellulose Structure, and Cellulose-Xylan Association on Biomethane Production

Methane production from XYm, XYs and WS is shown in Fig. 4a and Table 4. After 25 days of incubation, methane production reached its final level in all experiments (Fig. 4a), showing a difference in total accumulated biomethane from the XYm and XYs xylans. The methane potential of XYs (263 mL/g VS) was higher than that of XYm (240 mL/g VS). The variation in xylans biomethane potential could be attributable to the Ara/Xyl ratio; the lower the Ara/Xyl ratio, the higher the methane potential. Indeed, the degree, type and distribution pattern of the substitutions along the xylan backbone largely determine the structure and physical properties of xylan and have

Table 3 Assignment of different bands for lignin, cellulose and hemicellulose

Band (cm^{-1})	Assignment
3,500–3,000	O–H stretching
2,920–2,840	C–H stretching in –CH3 and –CH2-groups
1,750–1,680	C=O stretching in xylan
1,660–1,640	C=O stretching in conjugated ketones
1,515–1,505	C=C stretching from aromatic ring of lignin
1,470–1,460	C–H deformation in –CH3 and –CH2-groups
1,416–1,430	–CH2 vibration in cellulose
1,375–1,365	Aliphatic C–H stretching in –CH3
1,320–1,340	C–O vibration in S derivatives
1,270–1,256	C–O stretching in lignin "G -OMe groups"
1,245–1,210	C–C/C–O/C=O stretching in lignin and xylan
1,172–1,158	C–O-C Stretching at β-(1-4)-glycosidic
1,130–1,120	C=O/C–O–C stretching
1,060–1,050	C–O stretching in cellulose
1,040–1,030	C–O/C–C stretching in cellulose and xylan
900–896	C–O–C vibration at β-(1-4)-glycosidic
875–870	C–H in position 2, 5 and 6 (G units)

been shown to impact the enzymatic hydrolysis of xylan in the plant cell wall [38–40].

The digestion of cellulose nanowhiskers (WS) produced approximately 253 mL/g VS which is in the same range as the production from both xylan samples, though with a lower maximum rate and a higher lag-phase time (Table 4). The lower biomethane production rate of WS could be attributed to low bioavailability and accessibility of cellulose microfibrils to enzymes. This low accessibility could be due to the crystallinity and supramolecular organization of cellulose nanowhiskers. Furthermore, when XYm and XYs were incorporated into cellulose nanowhiskers, the digestion of holocelluloses fraction of whiskers-xylan "WS-XY" produced approximately 284 mL/g VS and 244 mL/g VS respectively (Table 4; Fig. 4b). However, the kinetic parameters of WS-XY nanocomposites varied in relation to xylan structure; for example the R_{max} of WS-XYm was higher than the R_{max} of WS-XYs (Table 4). The incorporation of XYm and XYs into the cellulose-WS matrix resulted in a reduction in the crystallinity index (Table 2). On the other hand, there was a difference in the Ara/Xyl ratio and *CrI* in the synthesized WS-XYs and WS-XYm nanocomposites [i.e. $CrI_{(WS\text{-}XYs)} > CrI_{(WS\text{-}XYm)}$ and $Ara/Xyl_{(WS\text{-}XYm)} > Ara/Xyl_{(WS\text{-}XYs)}$] (Table 2). According to Ara/Xyl values, WS-XYs BMP should be higher than WS-XYm BMP as was confirmed for the xylan polymers, though this is not the case for the xylans-nanowhiskers assemblies. However, *CrI* values correspond with the BMP values: the lower the *CrI*, the higher the methane potential. Consequently, the variation in biomethane potential of the WS-XY nanocomposites could be caused by the *CrI* of cellulose-WS microfibrils rather than by the hemicelluloses structure and Ara/Xyl ratio.

Influence of Lignin and Polysaccharides–Lignin Interaction on Biomethane Production

The anaerobic digestion of WS_{75}-LG_{25} produced approximately 268 mL/g VS and 339 mL/g WS whereas WS produced 253 mL/g WS (Table 4; Fig. 4b). Thus, lignin addition resulted in an increase in biomethane production from nanowhiskers associated with lignin (335 mL/g WS) versus nanowhiskers without lignin (253 mL/g of WS). This may be due to the decrease of cellulose crystallinity [$CrI_{(WS\text{-}LG)} < CrI_{(WS)}$]. The maximum rate of WS-LG anaerobic digestion also increased compared to that of nanowhiskers-WS (Table 4). However, the lag-time was slightly increased.

When methane production from both the 3-component (WS-XY-LG) nanocomposites and the nanocomposites without lignin (WS-XY) were compared, final methane production resulting from xylans and cellulose nanowhiskers proved not to be significantly affected by their interactions with lignin-G: (278 vs. 284 mL CH_4/g of carbohydrates for WS-XYm-LG and WS-XYm, respectively and 255 vs. 244 mL CH_4/g of carbohydrates for WS-XYs-LG and WS-XYs, respectively). Furthermore, higher methane production corresponded with the lowest crystallinity index and the highest ara/xyl ratio, as for WS-XY assemblies.

The impact of lignin structure on methane production can be observed by comparing WS-XYm-LG (containing only guïacyl–lignin) and WS-XYm-LGS (containing guïacyl and syringyl lignins). Final methane production was slightly higher (10 %) in LGS lignin. However, a more significant difference was observed in the digestion rate: R_{max} in WS-XYm-LGS was almost halved in comparison with WS-XYm-LG R_{max}. This difference in reactivity between cell wall-rich lignin-G and lignin-GS could lead to a better understanding of the digestibility of grass and woody plants. The only difference between G and S lignin monomers is the substitution by a methoxyl group in *ortho* position in lignin-S. The methoxyl group enables blocking inter-monomeric sites of coupling and modifies the electronic distribution. This ability to react favors the formation of β-O-4 linkages, which limit the ramification of chains and increases molecular weight and densification of the polymers formed in the case of lignin-S [41]. Consequently, a decrease in the digestion rate in the case of lignin-GS can be attributed to the high densification of lignin-GS nanoparticles and the strong interaction of lignin-GS to polysaccharides network, which limits the

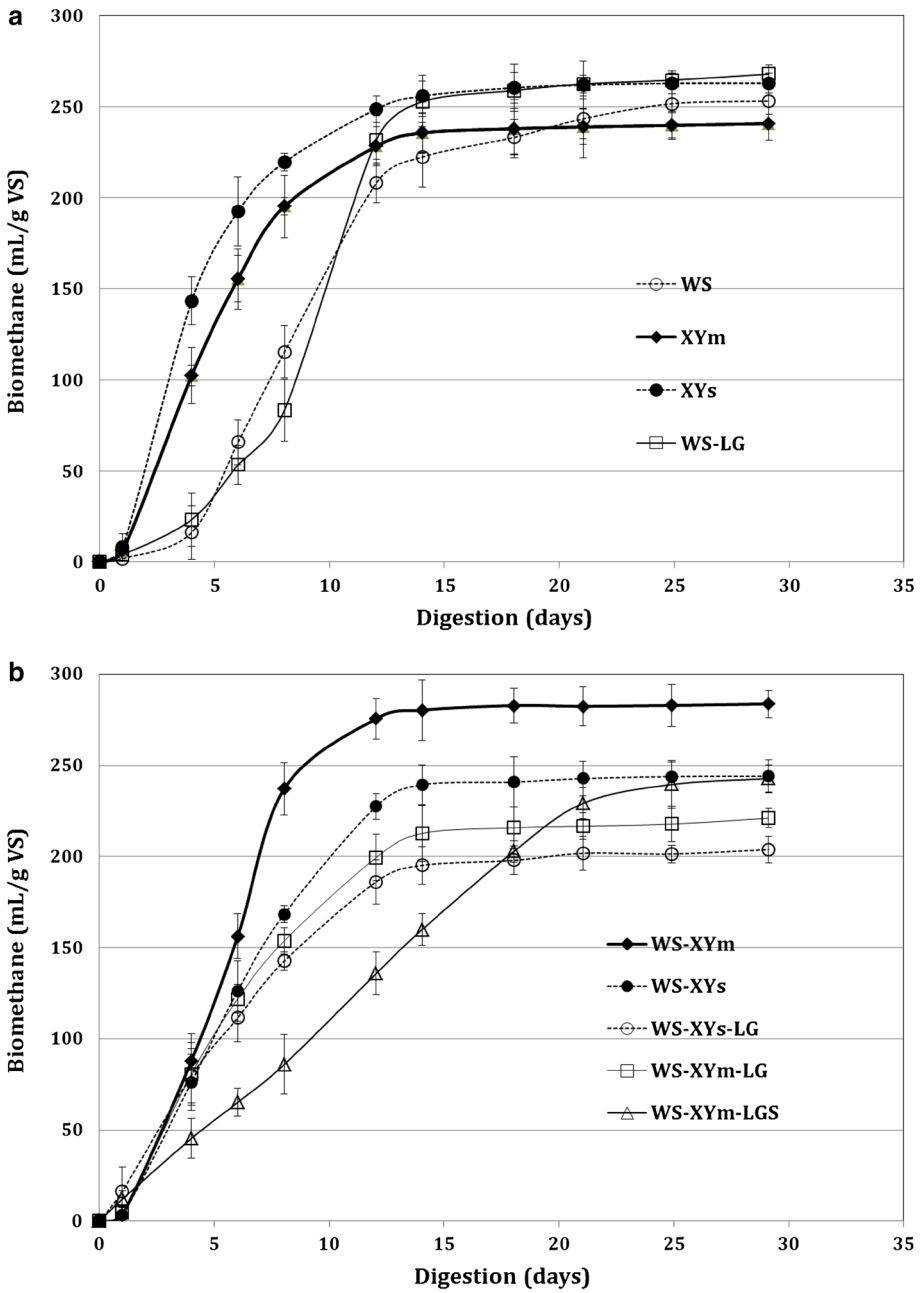

Fig. 4 Kinetics of methane production from **a** WS, XYm, XYs, and WS-LG; **b** WS-XYm, WS-XYs, and WS-XYs-LG, WS-XYm-LG and WS-XYm-LGS (mean value of duplicates $\pm 2 \times$ standard deviation)

accessibility of carbohydrates by enzymes. However, this point requires further in-depth investigation. On the other hand, the higher biomethane produced from lignin-GS could be a result of demethoxylation of the lignin polymer since methoxyl groups are more susceptible to biodegradation than side chain and aromatic ring structures (Fig. 1).

Figure 5 shows the microscopy images of anaerobic sludge with cellulose–xylan–lignin nanocomposite before and after anaerobic digestion. These images reveal that, after anaerobic digestion, the cellulose–xylan–lignin nanocomposites (Fig. 5b, c) present a different architecture and organization. They show the formation of composite lignin-rich "yellow spheres". The size of the lignin-rich nodules after anaerobic digestion was approximately 500 nm as compared to approximately 50 nm before anaerobic digestion. It has already been reported that lignin nodules and hydrophobic polymers in water display a similar shape and supramolecular organization. It appears that the degradation of carbohydrates in cellulose–xylan–lignin nanocomposites led to the reorganization and repolymerization of lignin-rich compounds which formed a dense, supramolecular complex structure with hydrophic properties i.e. "insoluble in water" and inaccessible to microorganisms.

Table 4 Methane production yields after 29 days of fermentation of whiskers, xylan and different nanocomposites and modified Gompertz equation parameters

Biocomposites	CH_4 (mL/g VS)	CH_4 (mL/g WS-XY)	Modified Gompertz equation parameter values			
			V_{max} (mL/gVS)	R_{max} (mL/gVS. d)	λ (day)	R^2
WS	253 ± 4	253	249 ± 3	29 ± 1	3.9 ± 0.2	0.998
XY_m	241 ± 3	241	239 ± 2	34 ± 1	1.2 ± 0.2	0.998
XYs	263 ± 5	263	259 ± 3	43 ± 3	0.9 ± 0.3	0.995
WS_{75}-XYm_{25}	284 ± 6	284	284 ± 3	44 ± 3	2.1 ± 0.2	0.997
WS_{75}-XYs_{25}	244 ± 7	244	245 ± 2	29 ± 1	1.6 ± 0.2	0.998
WS_{75}-LG_{25}	268 ± 7	339	269 ± 7	36 ± 5	5.1 ± 0.5	0.990
WS_{50}-XYm_{25}-LG_{25}	221 ± 5	282	219 ± 3	25 ± 2	1.1 ± 0.3	0.997
WS_{50}-XYm_{25}-$(LG_{50}S_{50})_{25}$	243 ± 5	307	263 ± 8	13.6 ± 0.7	1.6 ± 0.5	0.996
WS_{50}-XYs_{25}-LG_{25}	204 ± 6	259	203 ± 2	22 ± 1	0.7 ± 0.2	0.997

WS whiskers of cellulose, *XY* xylan, *LGS* Guiacyl/Syringyl lignin

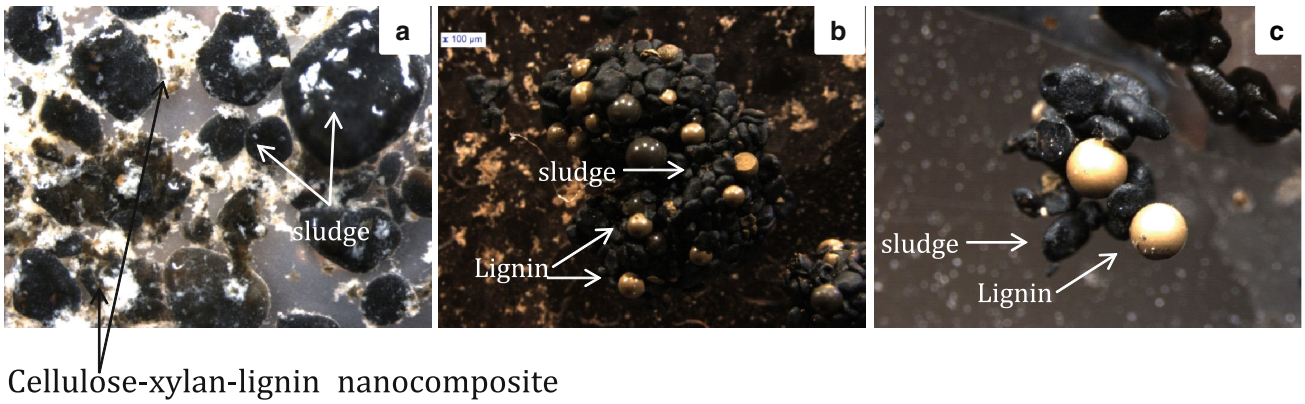

Fig. 5 Microscopic image of sludge (*black color*) with cellulose–xylan–lignin nanocomposite (*white color*), before anaerobic digestion (**a**), and after anaerobic digestion (**b**) and (**c**)

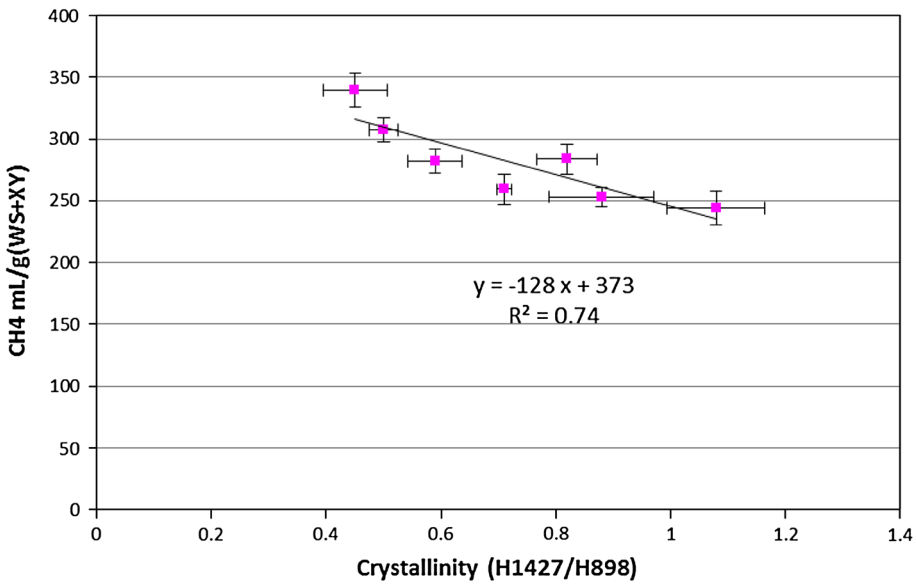

Fig. 6 Relationship between the methane potential of cellulose–xylan–lignin nanocomposites and the crystallinity defined as the ratio of the heights of FT-IR absorbance bands at 1,427 and 898 cm^{-1}

Relationship Between Substrates Physicochemical Properties and Biomethane Production

As mentioned in previous discussions, methane potential of various model nanocomposites seemed to be linked to cellulose crystallinity. Methane potential (mL/g carbohydrates) of the different model compounds containing cellulose was thus plotted versus the crystallinity index (H_{1427}/H_{898}) in Fig. 6. As already discussed, the general trend was a decrease in methane potential with an increase in H_{1427}/H_{898}. These results demonstrate that cellulose crystallinity is among one of the most important parameters concerning the anaerobic digestion of cellulose–xylan–lignin nanocomposites. Other studies have shown good correlations between the crystallinity and the rate of enzymatic hydrolysis of pure cellulose [42–45]. The progressive decrease in biomethane with an increase in CrI may be attributed to the limitation of cellulose bioavailability and accessibility to cellulolytic microorganisms when the substrate has a higher CrI. Recently, Rollin et al. [24] reported that in order to effectively release sugars from recalcitrant lignocellulose at high yield, the increase of cellulose accessibility was a more important pretreatment consideration than delignification.

This study clearly indicates that lignin content is not the sole parameter affecting the biodegradability of plant cell wall polysaccharides and biomethane production. Other factors, such as the cellulose crystallinity and crystalline polymorph, the surface area, porosity, lignin structure and lignin-carbohydrates complex may also play a significant role in the extent of lignocellulosic degradation.

Conclusions

This study concentrated on the anaerobic digestion of model cellulose whiskers, cellulose whiskers-xylans nanocomposites, cellulose whiskers-lignin and whiskers-xylans-lignin nanocomposites with constant lignin. Lignin-carbohydrates supramolecular organization was shown to play a significant role in lignocellulosic biomass anaerobic digestion. Lignin presence did not inhibit carbohydrate biodegradation but resulted in an increase in final methane production from a carbohydrate, which was linked to a decrease in the crystallinity index. Lignin presence also led to a decrease in the batch digestion rate; more so in the case of lignin-GS than lignin-G. These results will be valuable in the investigation of both anaerobic digestion of lignocellulosic biomass and biodegradability of plant cell-walls.

Acknowledgments The authors are grateful to Dr Kim Milferstedt for his help in microscopy analysis.

References

1. Salmen, L., Olsson, A.M.: Interaction between hemicelluloses, lignin and cellulose: structure-property relationships. J. Pulp Pap. Sci. **24**, 99–103 (1998)
2. Ebringerová, A., Heinze, T.: Xylan and xylan derivatives—biopolymers with valuable properties, 1. Naturally occurring xylans structures, isolation procedures and properties. Macromol. Rapid Commun. **21**, 542–556 (2000)
3. Sarkanen, K.V.: Precursors and their polymerization. In: Sarkanen, K.V., Ludwig, G.H. (eds) Lignins-Occurrence, Formation, Structure and Reaction, pp. 95–155. Wiley Interscience, New York (1971)
4. Vanholme, R., Morreel, K., Ralph, J., Boerjan, W.: Lignin engineering. In: Pauly, M., Keegstra, K. (eds) Current Opinion in Plant Biology Physiology and Metabolism, vol. 11, pp. 278–285. Current Biology LTD, London (2008)
5. Lapierre, C.: Application of new methods for the investigation of lignin structure. In: Jung, H.G., et al. (eds.) Forage Cell Wall Structure and Digestibility, pp. 133–163. American Society of Agronomy, Madison (1993)
6. Gunaseelan, V.N.: Biochemical methane potential of fruits and vegetable solid waste feedstocks. Biomass Bioenergy **26**, 389–399 (2003)
7. Murphy, J.D., Power, N.M.: An argument for using biomethane generated from grass as a biofuel in Ireland. Biomass Bioenergy **33**, 504–512 (2009)
8. Lubken, M., Gehring, T., Wichern, M.: Microbiological fermentation of lignocellulosic biomass: current state and prospects of mathematical modeling. Appl. Microbiol. Biotechnol. **85**, 1643–1652 (2010)
9. Barakat, A., Monlau, F., Steyer, J.P., Carrere, H.: Effect of lignin-derived and furan compounds found in lignocellulosic hydrolysates on biomethane production. Bioresour. Technol. **104**, 90–99 (2012)
10. Pavlostathis, S.G., Giraldogomez, E.: Kinetics of anaerobic treatment—a critical-review. Crit. Rev. Environ. Control **21**, 411–490 (1991)
11. Monlau, F., Barakat, A., Trably, E., Dumas, C., Steyer, J.P., Carrère, H.: Lignocellulosic materials into biohydrogen and biomethane: impact of structural features and pretreatment. Crit. Rev. Environ. Sci. Technol. **43**, 260–322 (2013)
12. Monlau, F., Sambusiti, C., Barakat, A., Trably, E., Guo, X.M., Latrille, E., Steyer, J.P., Carrère, H.: Predictive models of biohydrogen and biomethane based on the compositional and structural features of lignocellulosic materials. Environ. Sci. Technol. **46**, 12217–12225 (2012)
13. Taherzadeh, M.J., Karimi, K.: Pretreatment of lignocellulosic wastes to improve ethanol and biogas production: a review. Int. J. Mol. Sci. **9**, 1621–1651 (2008)
14. Chandler, J.A., Jewell, W.J., Gossett, J.M., Vansoest, P.J., Robertson, J.B.: Predicting Methane fermentation biodegradability. Biotechnol. Bioeng. **22**, 93–107 (1980)
15. Triolo, J.M., Sommer, S.G., Moller, H.B., Weisbjerg, M.R., Jiang, X.Y.: A new algorithm to characterize biodegradability of biomass during anaerobic digestion: influence of lignin concentration on methane production potential. Bioresour. Technol. **102**, 9395–9402 (2011)
16. Buffiere, P., Loisel, D., Bernet, N., Delgenes, J.P.: Towards new indicators for the prediction of solid waste anaerobic digestion properties. Water Sci. Technol. **53**, 233–241 (2006)
17. Benner, R., Maccubbin, A.E., Hodson, R.E.: Anaerobic biodegradation of the lignin and polysaccharide components of lignocellulose and synthetic lignin by sediment microflora. Appl. Environ. Microbiol. **47**, 998–1004 (1984)
18. Laureano-Perez, L., Teymouri, F., Alizadeh, H., Dale, B.E.: Understanding factors that limit enzymatic hydrolysis of biomass:

characterization of pretreated corn stover. Appl. Biochem. Biotechnol. **124**, 1081–1100 (2005)
19. Chang, V.S., Holtzapple, M.T.: Fundamental factors affecting biomass enzymatic reactivity. Appl. Biochem. Biotechnol. **84**, 5–37 (2000)
20. Gama, F.M., Mota, M.: Enzymatic hydrolysis of cellulose. 1. Relationship between kinetics and physico-chemical parameters. Biocatal. Biotransformation **15**, 221–236 (1997)
21. Ciolacu, D., Ciolacu, F., Popa, V.I.: Supramolecular structure—a key parameter for cellulose biodegradation. Macromol. Symp. **272**, 136–142 (2008)
22. Zhu, L., O'Dwyer, J.P., Chang, V.S., Granda, C.B., Holtzapple, M.T.: Structural features affecting biomass enzymatic digestibility. Bioresour. Technol. **99**, 3817–3828 (2008)
23. Galbe, M., Zacchi, G.: Pretreatment of lignocellulosic materials for efficient bioethanol production. In: Olsson, L. (ed.) Biofuels, pp. 41–65. Springer, Berlin (2007)
24. Rollin, J.A., Zhu, Z., Sathitsuksanoh, N., Zhang, Y.H.P.: Increasing cellulose accessibility is more important than removing lignin: a comparison of cellulose solvent-based lignocellulose fractionation and soaking in aqueous ammonia. Biotechnol. Bioeng. **108**, 22–30 (2010)
25. Barakat, A., Winter, H., Rondeau-Mouro, C., Saake, B., Chabbert, B., Catala, B.: Studies of xylan interactions and cross-linking to synthetic lignins formed by bulk and end-wise polymerization: a model study of lignin carbohydrate complex formation. Planta **226**, 267–281 (2007)
26. Grabber, J.H.: How do lignin composition, structure, and cross-linking affect degradability? A review of cell wall model studies. Crop Sci. **45**, 820–831 (2005)
27. Whitney, S.E.C., Brigham, J.E., Darke, A.H., Grand Reid, J.S., Gidley, M.J.: Structural aspects of interactions of mannan-based polysaccharides with bacterial cellulose. Carbohydr. Res. **307**, 299–309 (1998)
28. Tokoh, C., Takabe, K., Sugiyama, J., Fujita, M.: Cellulose synthesized by Acetobacter xylinum in the presence of plant cell wall polysaccharides. Cellulose **9**, 65–74 (2002)
29. Winter, H., Barakat, A., Cathala, B., Saake, B.: Preparation of arabinoxylan and its sorption on bacterial cellulose during cultivation. In: Fisher, K., Heinze, T. (eds) Makromolecular symposium series: hemicelluloses, pp. 85–92. Wiley-VCH, Wiesbaden, Germany (2006)
30. Touzel, J.-P., Chabbert, B., Monties, B., Debeire, P., Cathala, B.: Synthesis and characterization of dehydrogenation polymers in gluconacetobacter xylinus cellulose and cellulose/pectin composite. J. Agric. Food Chem. **51**, 981–986 (2003)
31. Ludley, F.H., Ralph, J.: Improved preparation of coniferyl and sinapyls alcohols. J. Agric. Food Chem. **44**, 2942–2943 (1996)
32. Hafren, J., Fujino, T., Itoh, T.: Changes in cell wall architecture of differentiating tracheids of *Pinus thunberghii* during lignification. Plant Cell Physiol. **40**, 532–541 (1999)
33. Uhlin, K.I., Atalla, R.H., Thompson, N.S.: Influence of hemicelluloses on the aggregation patterns of bacterial cellulose. Cellulose **2**, 129–144 (1995)
34. Xi, Y., Yasuda, S., Wu, H., Liu, H.: Analysis of the structure of lignin-carbohydrate complexes by the specific ^{13}C tracer method. J. Wood Sci. **46**, 130–136 (2000)
35. Parkas, J., Paulsson, M., Westermark, U., Terashima, N.: Solid state NMR analysis of b-13C-enriched lignocellulosic material during light-induced yellowing. Holzforschung **55**, 276–282 (2001)
36. Faix, O., Grunwald, C., Beinhoff, O.: Determinations of phenolic hydroxyl group content of Milled Wood Lignins from different botanical origins using selective aminolysis, FTIR, 1H-NMR and UV spectroscopy. Holzforchung. **46**, 425–532 (1992)
37. Collier, W.E., Schultz, T.P., Kalasinsky, V.F.: Infrared study of lignin—reexamination of aryl-alkyl ether C–O stretching peak assignments. Holzforschung **46**, 523–528 (1992)
38. Puls, J.: Chemistry and biochemistry of hemicelluloses: relationship between hemicellulose structure and enzymes required for hydrolysis. Macromol. Symp. **120**, 183–196 (1997)
39. Faulds, C.B., Mandalari, G., Lo Curto, R.B., Bisignano, G., Waldron, K.W.: Influence of the arabinoxylan composition on the susceptibility of mono- and dimeric ferulic acid release by *Humicola insolens* feruloyl esterases. J. Sci. Food Agric. **86**, 1623–1630 (2006)
40. Grabber, J.H., Ralph, J., Hatfield, R.D.: Ferulate cross-links limit the enzymatic degradation of synthetically lignified primary walls of maize. J. Agric. Food Chem. **46**, 2609–2614 (1998)
41. Barakat, A., Putaux, J.-L., Saulnier, L., Chabbert, B., Cathala, B.: Characterization of arabinoxylan-dehydrogenation polymer (synthetic lignin polymer) nanoparticles. Biomacromolecules **8**, 1236–1245 (2007)
42. Tarantili, P.A., Tarantili, P.A., Koullas, D.P., Christakopoulos, P., Kekos, D.: Cross-synergism in enzymatic hydrolysis of lignocellulosics: mathematical correlations according to a hyperbolic model. Biomass Bioenergy **10**, 213–219 (1996)
43. Jeihanipour, A., Karimi, K., Taherzadeh, M.J.: Enhancement of ethanol and biogas production from high-crystalline cellulose by different modes of NMO pretreatment. Biotechnol. Bioeng. **105**, 469–476 (2010)
44. Yoshida, M., Liu, Y., Uchida, S., Kawarda, K., Ukagami, Y., Ichinose, H., Kaneko, S., Fukuda, K.: Effects of cellulose crystallinity, hemicellulose, and lignin on the enzymatic hydrolysis of Miscanthus sinensis to monosaccharides. Biosci. Biotechnol. Biochem. **72**, 805–810 (2008)
45. Gupta, R., Lee, Y.Y.: Mechanism of cellulase reaction on pure cellulosic substrates. Biotechnol. Bioeng. **102**, 1570–1581 (2009)